Paper presented at the 22nd Asian Conference on Remote Sensing, 5 - 9 November 2001, Singapore.

Land Cover Classification Using NASA/JPL Polarimeric Synthetic Aperture Radar (POLSAR) Data

Ken Yoong LEE[1], Soo Chin LIEW[1], Leong Keong KWOH[1], Mikiyasu NAKAYAMA[2]

[1]Centre for Remote Imaging, Sensing and Processing
National University of Singapore
Block SOC1, Level 2
Lower Kent Ridge Road
Singapore 119260
Republic of Singapore
Tel: (65) 874 8029, Fax: (65) 775 7717, E-mail: crsleeky@nus.edu.sg

[2]United Graduate School of Agricultural Science
Tokyo University of Agriculture and Technology
3-5-8 Saiwai-cho, Fuchuu-city, Tokyo 183-8509
Japan
Tel: (81)-42-367-5667, Fax: (81)-42-360-7167

KEY WORDS: POLSAR, land cover, polarimetric filters, scattering mechanisms, complex Wishart classifier

ABSTRACT
This study intends to investigate the use of NASA/JPL POLSAR data (multilook C- and L-bands) for classifying land cover features, such as vegetation (i.e. grass, rice paddy, rubber), natural feature (i.e. river), and man-made features (i.e. canal, highway, runway, built-up area). Covering the area of Jitra, the 10 meters resolution air-borne POLSAR data acquired on 3 December 1996 was used in this study. Prior to the classification, the complex covariance matrix based Lee and Mean polarimetric filters were separately applied for evaluating their speckle suppression performance. In unsupervised classification, the scattering behavior of each pixel in Lee filtered images was analyzed, based on a multi-pixel algorithm and the phase difference. The supervised Wishart classifier was then used to reclassify the pixels of different scattering categories into the corresponding land cover classes. The Kappa statistics computed for both C- and L-band classified images were 0.73 and 0.76, respectively.

1. INTRODUCTION

Spaceborne remote sensing has long been an appropriate and effective data source for land cover mapping due to the wide coverage and repetitive observations (Haack and English, 1996). In general, there exist two major types of remotely sensed data: optical and synthetic aperture radar (SAR). Both optical and SAR data, however, have certain problems in their applications in mapping the tropical regions. The occurrence of extensive clouds is the main problem of the optical remote sensing data. As clouds interfere with the reception of optical sensors, its presence consequently causes the loss of land cover information in the captured data. At present, only single-frequency, single-polarization SAR is available on space-platforms. Land cover features cannot be significantly separated based on their single-band backscattering signature alone. Land cover classification using single-frequency single-polarization SAR data, hence, is not very successful. Nevertheless, with the advent of multifrequency and multipolarization SAR systems, the data captured has successfully attracted a great deal of attention in various applications (Boerner et. al, 1998). An attempt is made, in this study, to investigate and optimize the use of multifrequency and multipolarization SAR data for land cover classification over the tropical region. The main focus is placed on the C- and L-band NASA/JPL POLSAR data acquired during the Pacific Rim AIRSAR Campaign in 1996.

Sections 2 and 3 of this paper present the test area selected and the data acquired for this study. In Section 4, the speckle suppression and classification of POLSAR data are discussed. Section 5 analyzes the results obtained. Concluding remarks and recommendations are given in Section 6.

2. STUDY AREA

The test site identified for this study is an agricultural inland region covering an area of approximately 100 km^2 in the northwest of Peninsular Malaysia near Jitra (Figure 1a). It extends from 6° 11' to 6° 17' N latitude and 100° 21' to 100° 26' E longitude. The topography is characterized by flat and undulating terrain. The large portions of the site are the irrigated land, predominantly cultivated rice paddy. During the 1996 AIRSAR PacRim Deployment, the site was selected by the Malaysian Centre for Remote Sensing (MACRES) for land use and rice crop study (Lou et. al, 1997).

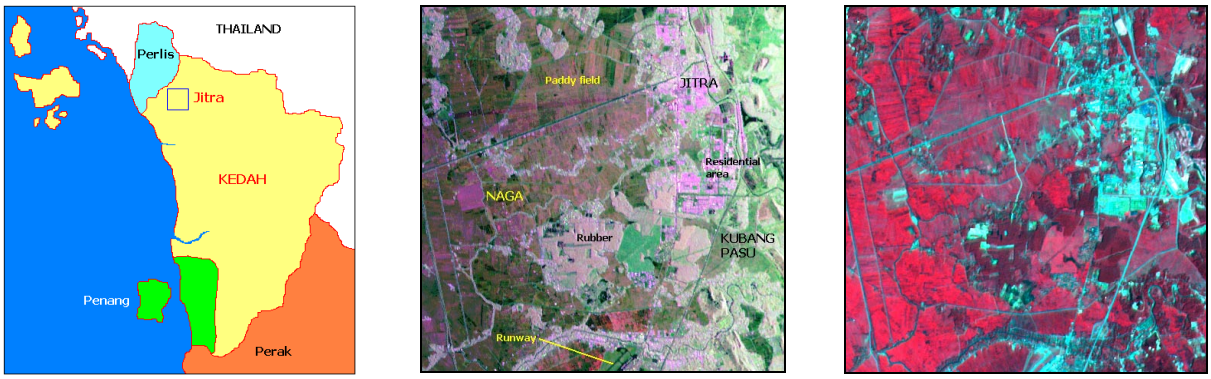

(a) (b) (c)

Figure 1: Location map of Jitra, Kedah (a) and the corresponding Lee polarimetric filtered (5×5) POLSAR data (b) as well as the multispectral SPOT-2 data (c)

3. DATA ACQUISITION

The data used in this study was provided by NASA/JPL. The POLSAR data, with C- (5.7 cm), L- (25 cm) and P- (68 cm) bands in full polarization (HH, HV, and VV), was acquired on 3 December 1996 using the AIRSAR instrument on-board a DC-8 aircraft. The aircraft flew at nearly 9 km altitude during data collection. The incidence angles were 24° for near range and 60° for far range corresponding to the near and far ranges of 10 and 20 km respectively. The 18-look POLSAR data supplied by NASA/JPL was projected into ground range with a ground pixel spacing of 10 meters. Only C- and L-bands (both in Compressed Stokes Matrix format) were examined in this study. A cloud-free SPOT-2 scene of the same area was also acquired and processed by CRISP, Singapore (Figure 1c). The 20-m resolution SPOT multispectral image was acquired on 1 January 1997 and processed to Level 2A. It was used together with the existing topographical and land use maps for locating the test sites.

4. METHODS AND IMPLEMENTATION

4.1 Speckle Suppression Using Polarimetric Filters

The POLSAR images (in complex covariance matrix form) were filtered using two polarimetric filters, namely Lee (Lee et. al, 1999b) and Mean (also known as "boxcar") filters. Window sizes of 3×3, 5×5, 7×7, were tested and analyzed. The performance of each polarimetric filter was assessed based on the criteria of Sheng and Xia (1996), i.e. speckle suppression index, SSI and edge enhancing index, EEI. The best filter should be capable of retaining linear land cover features (with higher EEI obtained) and homogenizing polygonal land cover features (with lower SSI obtained). Apart from the performance indicators, the absolute intensity difference of polarization signatures (extracted from the original and filtered images) was also computed to examine the filter's strength in preserving polarization properties. The smaller the intensity difference, the better the performance of the filter. Comparing both Lee and Mean filters (Figures 2 – 4), the former was found to be superior to the latter. Hence, the Lee filtered images of both C- and L-bands using 5×5 window were selected and employed in the subsequent classification process.

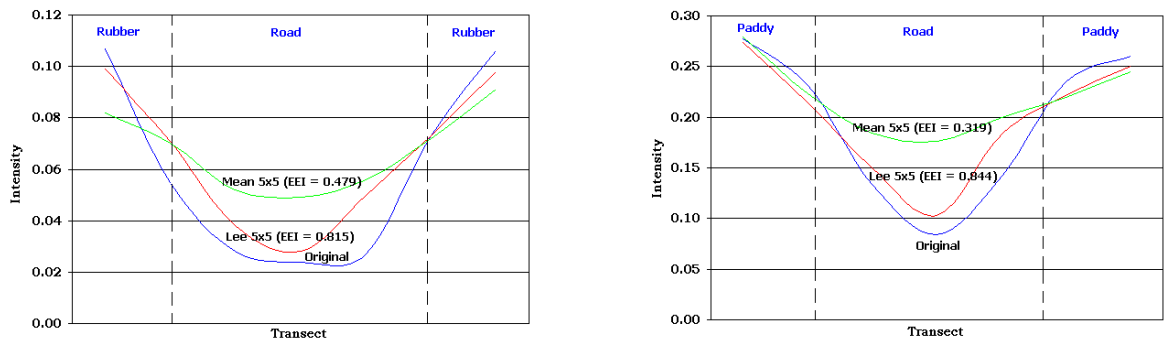

(a) (b)

Figure 2: One-dimensional intensity plot of road segment extracted from the L (a) and C (b) span images [span = $|HH|^2 + 2|HV|^2 + |VV|^2$]

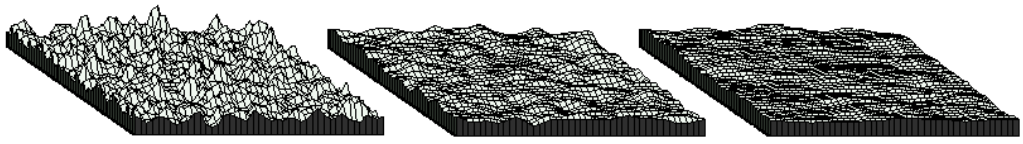

SSI = 0.357 SSI = 0.319

(a) Original **(b) Lee 5×5** **(c) Mean 5×5**

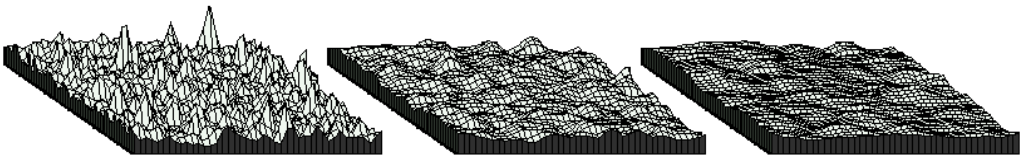

SSI = 0.382 SSI = 0.309

(d) Original **(e) Lee 5×5** **(f) Mean 5×5**

Figure 3: Three-dimensional intensity plot of rubber extracted from the C (a,b,c) and L (d,e,f) span images

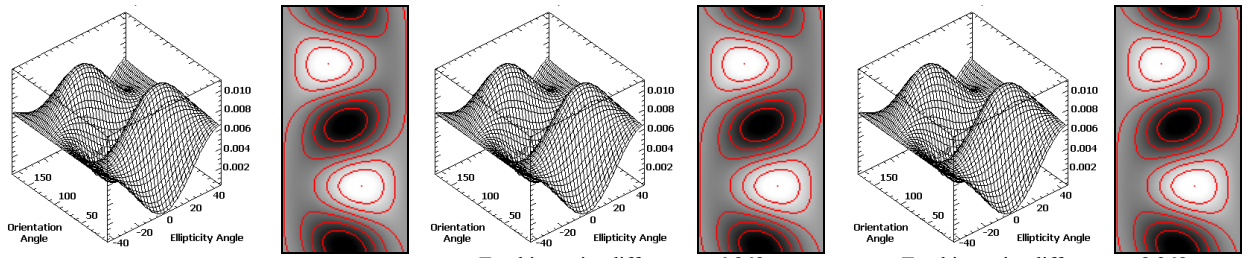

Total intensity difference = 6.868 Total intensity difference = 8.268

(a) Original **(b) Lee 5×5** **(c) Mean 5×5**

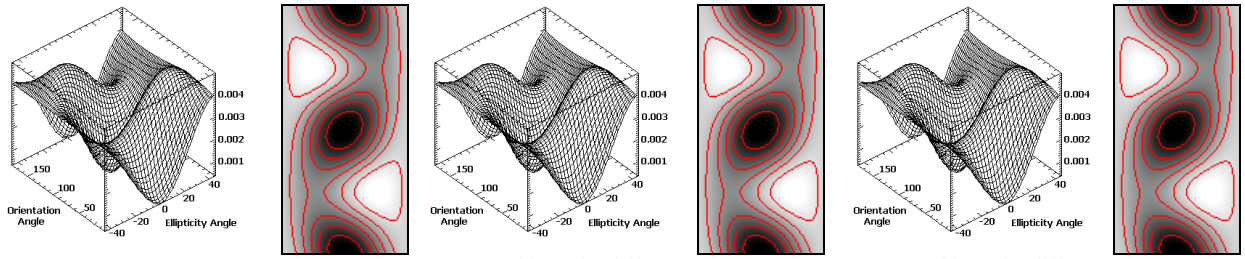

Total intensity difference = 4.791 Total intensity difference = 5.999

(d) Original **(e) Lee 5×5** **(f) Mean 5×5**

Figure 4: Polarization signature of paddy extracted from the L (a,b,c) and C (d,e,f) band data

4.2 Unsupervised Classification of Scattering Mechanisms

There are two different approaches of unsupervised classification carried out in this study. First, the multi-pixel classification algorithm proposed by Qong et. al (2000) – an improved version of van Zyl approach (1989) – was used to classify the Lee filtered image pixels into three categories: (1) odd number of reflections, (2) even number of reflections, and (3) diffuse scattering. To define the scattering behavior of each pixel, the classification involved the use of the elements of Muller matrix. Detailed discussions on the Muller matrix appear in van Zyl (1989) and Qong et. al (2000). Figures 5a and 5b show the classification outcomes of C- and L-bands where the odd-bounce, double-bounce, and diffuse scattering are colored in red, green, and blue respectively.

The phase difference between HH and VV polarization (ϕ_{HHVV}) was also studied and employed to group all pixels into (1) surface class where $|\phi_{HHVV}|<60°$, (2) $|\phi_{HHVV}|>120°$ for double-bounce class, and (3) unknown class (Lee et. al, 2001). Figures 5c and 5d give the C- and L-band classification outputs in which the surface, double-bounce, and unknown classes are presented in red, green, and white colors, respectively.

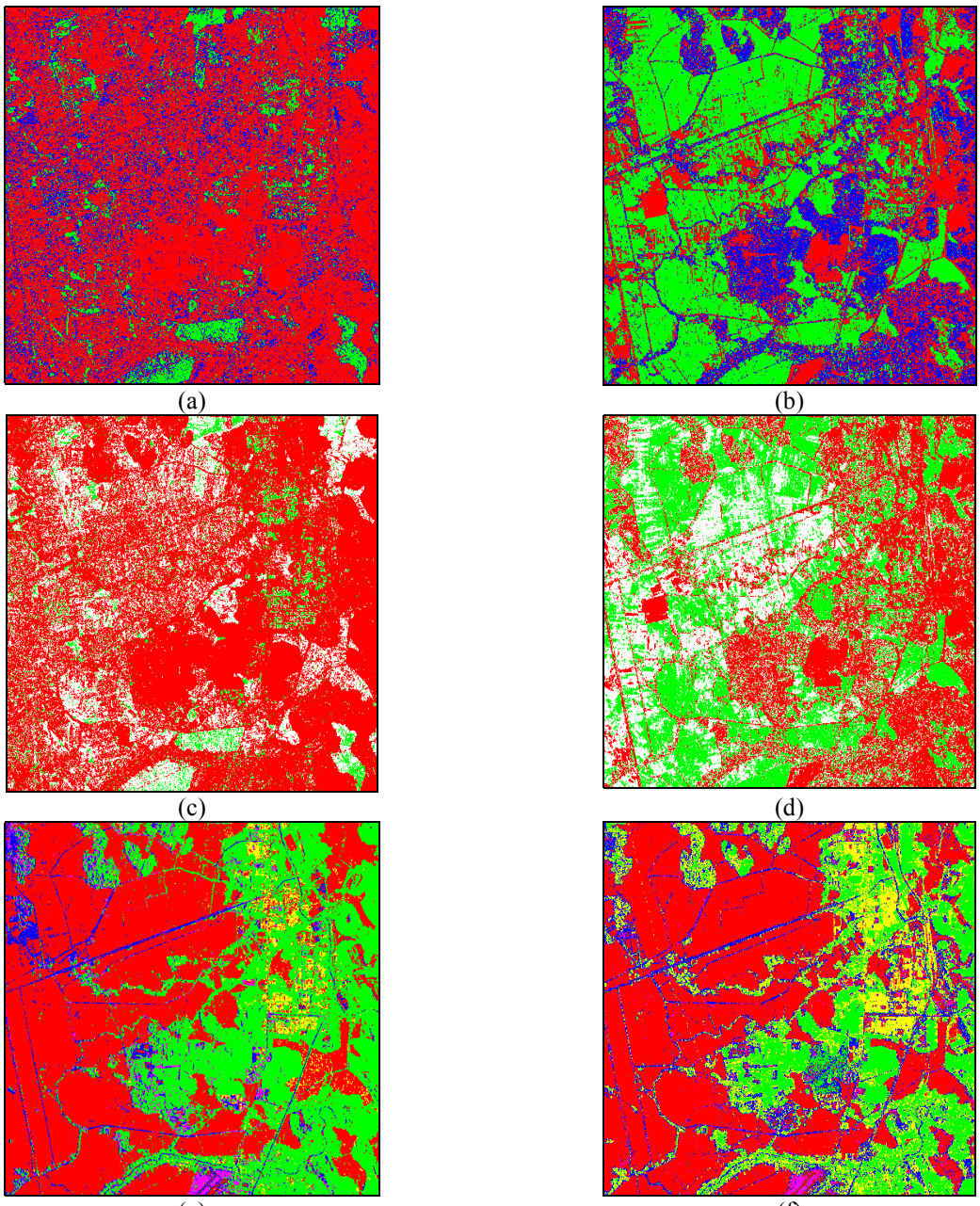

Figure 5: Unsupervised and supervised classification results of C- (a,c,e) and L- (b,d,f) band data. See text (Sections 4.2 and 4.3) for legends.

4.3 Supervised Classification Based on Complex Wishart Distribution

In supervised classification, the image pixels of different scattering classes, derived from the multi-pixel algorithm, were reclassified accordingly to the corresponding land cover categories by using the Bayesian Maximum Likelihood classifier (Lee et. al, 1999a; 1994). The complex coherency matrix $\boldsymbol{T}$ (a Hermitian matrix) of candidate pixel $\boldsymbol{P}$, which is based on Pauli matrix representation, was used to compute its distance to each target class $\boldsymbol{m}$. The distance measure is defined by

$$d(\boldsymbol{T},\boldsymbol{V_m}) = \mathrm{In}|\boldsymbol{V_m}| + \mathrm{Tr}(\boldsymbol{V_m}^{-1}\boldsymbol{T}) \qquad (1)$$

where $\boldsymbol{V_m}$ is the mean coherency matrix for target class $\boldsymbol{m}$. The pixel $\boldsymbol{P}$ is assigned to the target class with the minimum distance measured. Figures 5e and 5f present the classification results of C- and L-band images [paddy (red), rubber (green), built-up area (yellow), grassland (magenta), runway (brown), water (blue)]

5. RESULTS AND DISCUSSION

As can be seen in Figure 5b, the paddy and built-up area in L-band data were categorized by the multi-pixel algorithm into the even-bounce class whilst the rubber was dominated by diffuse scattering. The canal, grassland, highway, river, and runway which exhibit specular scattering fell into the odd-bounce class. For the classification based on ϕ_{HHVV}, the L-band classified result was identical to that of using the multi-pixel algorithm, except for the rubber class. The rubber was classified into the surface class. For the C-band data, all land cover features, excluding built-up area, were characterized by the multi-pixel algorithm and phase difference as having the odd-bounce scattering behavior. Table 1 presents the scattering mechanisms of land cover classes of both C- and L-band data. In this study, it was found that the multi-pixel algorithm yielded more satisfying and detailed results than that based purely on the phase difference. The total unclassified pixels in the phase difference based classified images were 23% and 29% for the C- and L-bands, respectively.

Table 1: Scattering mechanisms (in percent) of each land cover class

Land cover	Band	Scattering classes based on multi-pixel algorithm			Scattering classes based on phase difference		
		Odd-bounce	Even-bounce	Diffuse scattering	Surface	Double-bounce	Unknown
Grassland	C	**93.93**	-	6.07	**97.66**	1.06	1.28
	L	**100**	-	-	**98.54**	-	1.46
Paddy	C	**78.81**	15.99	5.20	**55.21**	10.78	34.01
	L	3.79	**94.57**	1.64	-	**80.99**	19.01
Rubber	C	**98.86**	-	1.14	**98.44**	-	1.56
	L	5.43	10.66	**83.91**	**48.89**	23.70	27.41
River	C	**97.43**	-	2.57	**100**	-	-
	L	40.94	5.89	**53.17**	**97.65**	-	2.35
Canal	C	**85.09**	4.13	10.78	**95.66**	-	4.34
	L	**98.56**	-	1.44	**97.21**	-	2.79
Highway	C	**98.72**	-	1.28	**100**	-	-
	L	**98.93**	-	1.07	**99.31**	-	0.69
Runway	C	**96.67**	-	3.33	**100**	-	-
	L	**100**	-	-	**99.23**	-	0.77
Built-up area	C	40.40	**43.15**	16.45	42.43	**46.90**	10.67
	L	18.05	**70.93**	11.01	19.03	**59.93**	21.04

For the C- and L-band supervised classified images, the overall accuracy and Kappa statistics (Arora and Ghosh, 1998) were computed and are tabulated in Table 2. The classification results obtained were promising where the correct classification of land cover classes was more than 70% for both C- and L-bands. With the longer wavelength, the L-band data shows more distinct discrimination between land cover classes and thus gives the better classification performance compared to the C-band. From Figures 5e and 5f, it was clearly observed that the highway was misclassified into the waterbody class due to their poor separation. Table 3 gives the separation of the land cover classes computed based on Lee et. al (1999a). The separation measure was computed as

$$R_{ij} = \frac{D_{ii} + D_{jj}}{D_{ij}} \tag{2}$$

where D_{ii} and D_{jj} represent the dispersion within class, D_{ij} denotes the distance between classes i and j. The large measured value of R_{ij} indicates the poor separability of the two classes.

6. CONCLUSIONS AND RECOMMENDATION

The C- and L-band POLSAR data have proven to be useful in land cover classification, especially for paddy class. An overall accuracy of 80% was shown by the L-band whilst the accuracy achieved by C-band was 78%. For future study, it is recommended that the classification of POLSAR data can include some additional information, such as texture statistics (Mancini and Griffths, 1992), polarimetric discriminators (Touzi et. al, 1992), and decomposition elements (Cloude and Pottier, 1997) in order to improve the accuracy.

Table 2: Classification accuracy computed from C- and L-band POLSAR images

	Percent of correct classified into						Overall accuracy	Kappa statistics
	Paddy	Rubber	Built-up area	Grassland	Runway	Waterbody*		
C-band	80.78	83.59	73.44	79.18	75.00	70.82	**78.18**	**0.7315**
L-band	87.65	80.12	85.83	72.55	74.03	71.09	**80.74**	**0.7552**

*Canals and river are categorized as waterbody

Table 3: Separation measured between highway, canal, river, and runway in C- and L-band data

	Highway versus canal	Highway versus river	Highway versus runway
C-band	3.395	2.840	-3.601
L-band	2.968	2.885	-5.168

ACKNOWLEDGEMENT

NASA/JPL is gratefully acknowledged for providing the POLSAR data. The fourth author (M. Nakayama) acknowledges partial support from NASDA ALOS project.

REFERENCES

Arora, M. & Ghosh, S. K., 1998. Classification Accuracy Indices: Definitions, Comparisons and a Brief Review. Asian-Pacific Remote Sensing and GIS Journal, 10(2), pp. 1-9.

Boerner, W.-M., Mott, H., Luneburg, E., Livingstone, C., Brisco, B., Brown, R. J., Paterson, J. S., Cloude, S. R., Krogager, E., Lee, J. S., Schuler, D. L., van Zyl, J. J., Randall, D., Budkewitsch, P., & Pottier, E., 1998. Polarimetry in Radar Remote Sensing: Basic and Applied Concepts. In: Manual of Remote Sensing - Principles and Applications of Imaging Radar, edited by Henderson, F. M. & Lewis, A. J., John Wiley & Sons, Inc., The United States of America, pp. 271-357.

Cloude, S. R. & Pottier, E., 1997. An Entropy Based Classification Scheme for Applications of Polarimetric SAR. IEEE Transactions on Geoscience and Remote Sensing, 35(1), pp. 68-78.

Haack, B. & English, R., 1996. National Land Cover Mapping by Remote Sensing. World Development, 24(5), 845-855.

Lee, J. S., Grunes, M. R. & Kwok, R., 1994. Classification of Multi-look Polarimetric SAR Imagery Based on Complex Wishart Distribution. International Journal of Remote Sensing, 15(11), pp. 2299-2311.

Lee, J. S., Grunes, M. R., Ainsworth, T. L., Du, L.-J., Schuler, D. L. & Cloude, S. R., 1999a. Unsupervised Classification Using Polarimetric Decomposition and the Complex Wishart Classifier. IEEE Transactions on Geoscience & Remote Sensing, 37(5), pp. 2249-2258.

Lee, J. S., Grunes, M. R. & de Grandi G., 1999b. Polarimetric SAR Speckle Filtering and Its Implication for Classification. IEEE Transactions on Geoscience & Remote Sensing, 37(5), pp. 2363-2373.

Lee, J. S., Grunes, M. R., Pottier, E. & Ferro-Famil, L., 2001. Segmentation of Polarimetric SAR Images. Presented in IEEE International Geoscience and Remote Sensing Symposium.

Lou, Y., Kim, Y., van Zyl, J. J., Maldonado, L., Miller, T., O'Leary, E., Romero, G., Skotnicki, W. & Taylor, V., 1997. The NASA / JPL Airborne Synthetic Aperture Radar's 1996 PacRim Deployment. In: IEEE International Geoscience and Remote Sensing Symposium Proceedings, Vol3, pp. 1404-1406.

Mancini, P. & Griffiths, H. D., 1992. Texture Analysis in Polarimetric SAR Using the Covariance Matrix. In: IEEE International Geoscience and Remote Sensing Symposium Proceedings, Vol2, pp. 893-895.

Sheng, Y. & Xia, Z.-G., 1996. A Comprehensive Evaluation of Filters for Radar Speckle Suppression. In: IEEE International Geoscience and Remote Sensing Symposium Proceedings, Vol3, pp. 1559-1561.

Qong, M., Tadono, T., Wakabayashi, H. & Shimada, M., 2000. Muller Matrix Based on Classification of Polarimetric SAR Data. In: IEEE International Geoscience and Remote Sensing Symposium Proceedings, Vol1, pp. 375-377.

Touzi, R., Goze, S., Le Toan, T., Lopes, A. & Mougin, E., 1992. Polarimetric Discriminators for SAR Images. IEEE Transactions on Geoscience and Remote Sensing, 30(5), pp. 973-980.

van Zyl, J. J., 1989. Unsupervised Classification of Scattering Behavior Using Radar Polarimetry Data. IEEE Transactions on Geoscience & Remote Sensing, 27(1), pp. 36-45.